

# Deep Kernelized Dense Geometric Matching

Johan Edstedt<sup>1</sup> Mårten Wadenbäck<sup>1</sup> Michael Felsberg<sup>1</sup>

## Abstract

Dense geometric matching is a challenging computer vision task, requiring accurate correspondences under extreme variations in viewpoint and illumination, even for low-texture regions. In this task, finding accurate global correspondences is essential for later refinement stages. The current learning based paradigm is to perform global fixed-size correlation, followed by flattening and convolution to predict correspondences. In this work, we consider the problem from a different perspective and propose to formulate global correspondence estimation as a continuous probabilistic regression task using deep kernels, yielding a novel approach to learning dense correspondences. Our full approach, **Deep Kernelized Matching**, achieves significant improvements compared to the state-of-the-art on the competitive HPatches and YFCC100m benchmarks, and we dissect the gains of our contributions in a thorough ablation study.

## 1. Introduction

Finding pixel-wise correspondences between pairs of images is a fundamental computer vision problem with numerous important applications, including 3D reconstruction (Schonberger & Frahm, 2016), SLAM (Mur-Artal et al., 2015), image registration (Shrivastava et al., 2011), visual re-localisation (Lynen et al., 2020), and semantic transfer (Kim et al., 2019). Dense correspondence estimation has most commonly been addressed in the context of optical flow (Horn & Schunck, 1981), where the image pairs represent consecutive frames in a video and viewpoint and illumination differences are typically small. In this work we will consider the general task of learning *dense geometric matching*, finding all correspondences between an arbitrary image pair of a 3D scene. In contrast to optical flow, image pairs in this task may exhibit extreme variations

in viewpoint (Li & Snavely, 2018), illumination (Balntas et al., 2017), and even season (Toft et al., 2020). Due to the complexity of the task, it has only in the recent deep learning era received an increased interest (Rocco et al., 2017; Melekhov et al., 2019; Shen et al., 2020; Truong et al., 2020b; Wiles et al., 2021; Jiang et al., 2021).

Arguably, the most important step in dense geometric matching is the initial extraction of global correspondences. A popular method is to perform global matching, i.e. computing similarities for all possible pairs, from which correspondences can be extracted. In sparse geometric matching, typically (soft) mutual nearest neighbours (Rocco et al., 2018) are used as a heuristic. However, for dense matching this is not feasible, as each pixel must be assigned a match. In previous works (Rocco et al., 2017; Melekhov et al., 2019; Truong et al., 2020b), the global correspondences are simply flattened into a vector, and processed by a CNN decoder directly. This is unsatisfactory, as it ignores the local structure, and forces the network to use a fixed size resolution.

A recent work by Truong et al. (2020a) somewhat remedies this issue by first employing internal optimization on the global correlation, before it is fed into the decoder, while others (Teed & Deng, 2020; Huang et al., 2021) use iterative procedures to query the correlation volume or use robust parametric estimators (Shen et al., 2020) on all putative correspondences to align the pair.

In this work we propose a different view of correspondence extraction, that bypasses the issues above by reformulating the dense correspondence problem through the lens of probabilistic regression. Specifically, we will view matching as a regression problem from feature to coordinate space, that is resolution independent and respects the geometric structure. Furthermore, to discern multimodal matches from intermediate matches, we introduce coordinate embeddings and incorporate them into the regression framework. To decode these mappings, we use a convolutional decoder to directly decode the embedded coordinates. This decoder can both enforce the *local coherence* (Yuille & Grzywacz, 1988), i.e. the tendency for neighbouring pixels to move together, and decode the embedded coordinates to back to natural coordinates. Finally, to fine-tune the matches and get sub-pixel accuracy, we propose a multi-scale regressive convolutional

<sup>1</sup>Computer Vision Laboratory, Department of Engineering, Linköping University. Correspondence to: Johan Edstedt <johan.edstedt@liu.se>.

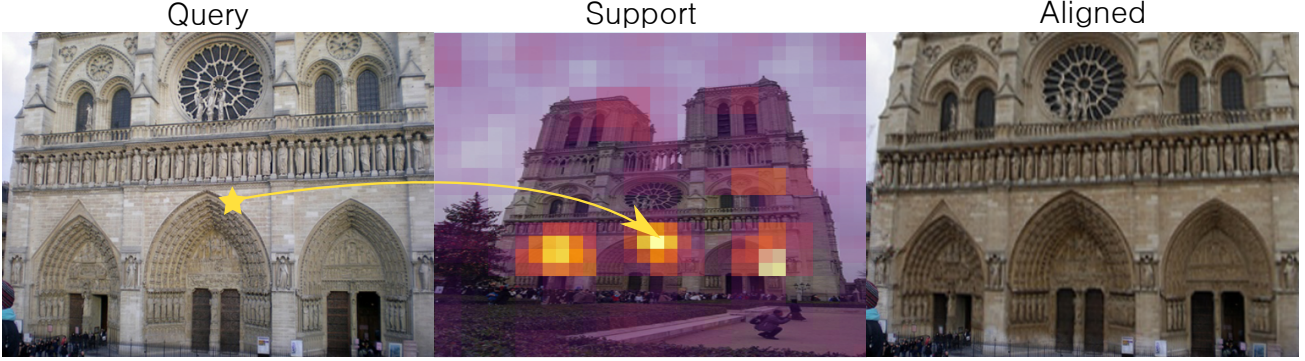


Figure 1. Illustration of our full approach on the challenging YFCC100m (Thomee et al., 2016) benchmark. Shown to the left and in the middle is the correlation between the embedded support coordinate predicted by our probabilistic regressor, and the embedded support grid. Notably, the prediction is tri-modal with the dominant mode at the correct match. To the right, the final predicted dense warp  $\hat{\omega}$  between query and support image by our model is shown, using the predicted confidence of the model to blend. Our model is able to reason about both uncertainty and multimodality through our formulation, and our approach sets a new state-of-the-art on both the HPatches and YFCC100m benchmarks.

refiner, that processes both images jointly through warping. We illustrate our approach in Figure 1.

Our proposed method achieves an impressive improvement of 4% AUC@5° compared to the previous best performing method on the YFCC100m pose estimation benchmark, and a significant improvement of 4% PCK-1 on the dense matching benchmark HPatches. Finally, our method makes a remarkable gain of over 20% PCK-1 on the sparse HPatches benchmark compared to the best performing previous method, indicating the superiority of dense methods compared to sparse methods for sub-pixel performance.

**Contributions** Our contributions are as follows. First, we formulate global correlation and correspondence extraction as a feature-vector to coordinate probabilistic regression task. Secondly, we extend the regression task to embedded coordinate spaces. Lastly, we propose a coordinate decoder and a multiscale refinement module.

## 2. Related Work

**Dense Matching** Dense correspondence estimation has its roots in image registration (Lucas & Kanade, 1981) and optical flow (Horn & Schunck, 1981). The early methods typically assumed small displacements and the *brightness constancy* assumption, often formulated as a variational problem. Black & Anandan (1996) introduced piecewise parametric models to deal with occlusions and discontinuities, Brox & Malik (2010) extended the variational methods to cases with large displacements, and Liu et al. (2010) tackled flows between visually distinct scenes. In the deep learning era, optical flow has received much attention, with FlowNet (Dosovitskiy et al., 2015; Ilg et al., 2017) and multiple subsequent works (Sun et al., 2018; Hur & Roth,

2020; Teed & Deng, 2020). Closer to our work, there has recently been increased interest in dense geometric matching (Rocco et al., 2017; Melekhov et al., 2019; Laskar et al., 2020; Shen et al., 2020; Truong et al., 2020b;a; 2021b;a;c; Wiles et al., 2021; Jiang et al., 2021). The main difference in our method compared to these works is the probabilistic embedded coordinate regression view of global matching, and the associated embedding decoder.

**Establishing Geometric Correspondences** Geometric matching has traditionally been performed sparsely by key-point detection and description (Lowe, 2004; Dalal & Triggs, 2005; Bay et al., 2006; Dusmanu et al., 2019; Revaud et al., 2019; DeTone et al., 2018; Luo et al., 2019; Tyszkiewicz et al., 2020; Wang et al., 2020). Here a sparse set of points are matched between images based on some matching criterion, typically mutual nearest neighbours (Dusmanu et al., 2019; Revaud et al., 2019). The matching of sparse correspondences has recently received increased interest with Neighbourhood Consensus Networks (Rocco et al., 2018; 2020; Zhou et al., 2021), SuperGlue (Sarlin et al., 2020), and LoFTR (Sun et al., 2021), showing promising results.

For dense geometric correspondences the earliest learned method by Rocco et al. (2017) used the flattened global correlation volume to produce the parameters of a parametric geometric transformation. Following works (Melekhov et al., 2019; Truong et al., 2020b), instead moved toward individual pixel offsets. Recently Truong et al. (2020a) propose an internal optimization procedure on the global correlation, to improve the subsequent decoding steps.

**Channel Decoding and Motion Coherence** Our convolutional decoder can be seen as a combination of channel decoding (Campbell & Robson, 1968; Pouget et al., 2000;

Forssén, 2004; Jonsson & Felsberg, 2009; Felsberg et al., 2012) of embedded coordinates and robustification/local coherence (Yuille & Grzywacz, 1988; Weiss & Adelson, 1998) of a vector field. Utilizing local coherence is particularly important for dense matching, since the local signal may often be intrinsically 0-D or 1-D, often referred to as the aperture problem (Wohlgemuth, 1911; Wallach, 1935; Adelson & Movshon, 1982).

Recently, vector field robustification for geometric matching was considered by Ma et al. (2014) and by Bian et al. (2017), by minimizing a regularized objective over functions in RKHS from putative correspondences in coordinate space. Some other methods could also be considered to be robustification techniques, such as the works of Brachmann & Rother (2019), and Yi et al. (2018) where coordinate correspondences are processed directly by a neural network to produce match likelihoods. The enforcement of local coherence was also discussed by Rocco et al. (2018), although it was there referred to as *neighbourhood consensus* with some following works (Li et al., 2020; Rocco et al., 2020).

**Deep Kernels and Gaussian Processes** Deep kernels (Wilson et al., 2016), and their associated GPs, were at first used as an alternative to SGD training in classification and regression. Some later works extend this notion to few-shot classification (Patacchiola et al., 2020; Snell & Zemel, 2021; Wang et al., 2021). In this work we use deep kernels to infer functions from feature-vectors to (some embedding of) spatial coordinates, which has hitherto not been explored. We additionally combine the GPs with a convolutional decoder.

Concurrently with our work, Johnander et al. (2021) consider the few-shot segmentation task as a mapping between feature-vectors and learned embeddings of binary segmentation masks and apply GP regression. However, their task is semantic, and hence the pixel-precision is of little importance. In this work we show how to extend neural network embedded deep kernels to geometric matching, which requires pixel-level precision.

**Cross-Attention** While we focus on GPs, cross-attention bears multiple similarities. Sun et al. (2021) use cross-attention in conjunction with positional encodings to predict correspondences. However, they do not consider dense-matching but rather employ a sparsification scheme, with mutual nearest neighbour matching. We further discuss the similarities and differences between cross-attention and GPs in Section 3.2.

### 3. Method

#### 3.1. Preliminaries

Consider two images  $\mathbf{I}_Q, \mathbf{I}_S$  (query and support), on image coordinate grids  $\mathbf{X}_Q, \mathbf{X}_S$  of a 3D scene. In general we

will assume a natural coordinate system for both images as  $[-1, 1] \times [-1, 1]$ . For these images we extract feature vectors with some encoder,  $\phi_Q = F(\mathbf{I}_Q), \phi_S = F(\mathbf{I}_S)$ . We will consider the general task of mapping each pixel in the query image, with a pixel in the support image, such that both relate to the same 3D-point in the scene. Notwithstanding ill-posedness, e.g. occlusions and low-texture regions, we will assume that such a mapping exists. The general task can be framed as  $\omega_{Q \rightarrow S} : \mathbb{X}_Q \rightarrow \mathbb{X}_S$ , where  $\omega$  warps the coordinates in the query image to the support. Additionally we will explicitly predict the valid regions of the mapping as  $\hat{p}(\mathbf{X}_Q)$ , where the reference  $p(\mathbf{X}_Q)$  is obtained, e.g., by consistent depth.

While the full task could be considered atomically, we split it into two steps. In the first step, we are interested in finding functions  $\Lambda : \Phi \rightarrow \mathbb{E}_S$ , where  $\Phi$  is the feature vector space and  $\mathbb{E}_S$  is an embedding space of the spatial coordinates. Here we may condition on the features and spatial coordinates from the support image ( $\phi_S, \mathbf{E}_S$ ).

Once a function  $\Lambda$  has been estimated, with some abuse of notation, we associate the query grid with the query features and view  $\Lambda$  as a function of the query coordinates, i.e.  $\Lambda(\phi_Q(\mathbf{X}_Q))$ . The second step then consists of decoding  $\Lambda$  to the estimated warping function, i.e.  $\hat{\omega}_{Q \rightarrow S} := D(\Lambda(\mathbf{X}_Q))$ , where  $D$  is the neural decoder.

In the following sections we will describe our approach for constructing  $\Lambda$  and  $D$ .

#### 3.2. Constructing $\Lambda$

A simple approach to constructing  $\Lambda$  is **nearest-neighbour(s)**. Given the feature vectors and coordinates in the support image we let the corresponding feature vectors in the query image be associated with the coordinates of the closest (given some metric) feature vector. This results in piece-wise constant functions, which may or may not be desired. It further imposes difficulties in gradient propagation, as the derivative is 0 a.e.

An alternative approach is to use **cross-attention**, with some appropriate kernel, that creates functions as linear combinations of the support set, i.e.

$$\Lambda(\phi; \mathcal{S}) = \frac{\sum_{s \in \mathcal{S}} k(\phi, \phi_s) e_s}{\sum_{s \in \mathcal{S}} k(\phi, \phi_s)}.$$

It can be seen that this (for an appropriate choice of kernel) is exactly<sup>1</sup> kernel smoothing, as was previously noted by Tsai et al. (2019). Properties of kernel smoothers are well-known and in general the resulting functions are well behaved. However, they face difficulties in situations where the support set is non-uniformly dense, or where the local

<sup>1</sup>Multi-head attention can be seen as a linear combination of kernel smoothers.

curvature is strong, e.g. near object boundaries (Häger et al., 2021). Furthermore, they do not provide any uncertainty estimates. Some previous work in correspondence learning can be viewed in this light, e.g. (Sun et al., 2021; Wiles et al., 2021; Jiang et al., 2021), although the kernel smoother connections were not discussed there. For further reading on kernel smoothers see, e.g., Friedman et al. (2001).

In our approach we will consider **GP regression** as a suitable candidate. Here the output  $\phi$  is considered as random variables, and the main assumption being that these are jointly Gaussian. A GP is uniquely<sup>2</sup> defined by its kernel  $k$ , that must be a positive-definite function. The kernel can be seen as a continuous generalization of a covariance matrix, and is hence often called a covariance function. Under these conditions, there are analytic formulae for the posterior of functions, given the support set. The posterior can be written as

$$\begin{cases} \mu(\phi_Q) = K_{QS} K_{SS}^{-1} E_S, \\ \Sigma(\phi_Q) = K_{QQ} - K_{QS} K_{SS}^{-1} K_{SQ}, \end{cases}$$

where  $K$  denotes the kernel matrix,  $\mu$  is the posterior mean function, and  $\Sigma$  is the posterior covariance.

There are multiple ways of constructing  $\Lambda$  from the posterior. A simple way is to set  $\Lambda = \mu$ . We found concatenating  $\mu$  and local neighbourhood of  $\Sigma$  to work well in practice, other approaches could also be taken, e.g. sampling, although that is beyond the scope of this paper.

GPs provide multiple benefits. They elegantly handle non-uniform densities, give useful covariance estimates, and enable extensive flexibility and interpretability through the choice of kernel. For a more complete overview of GPs we refer to Rasmussen & Williams (2005). For some intuition regarding the above approaches, we provide a toy-example in appendix A.2

While attractive, the feature-to-coordinate view struggles with *multi-modality*. Whenever similar features map to different coordinates, the regressive model predicts *something in between*. If this cannot be distinguished from the intermediate coordinate, there will be ambiguity in the decoding. We will call these ambiguities *metamers*, following the terminology of (Snippe & Koenderink, 1992). This problem will be dealt with next.

**Positional Embeddings** To reduce the metamer problem, we may choose an *embedding space* for our coordinates. Crucially, this embedding must be non-linear, simply due to the fact that the metamers otherwise remain.

We will consider the following embedding, which is a common choice (Rahimi & Recht, 2007; Tancik et al.; Sun et al., 2021),

$$\mathbf{B}_{\mathcal{F}}(x; W, b) = \cos(Wx + b),$$

<sup>2</sup>With the common assumption that the mean function is 0.

where  $W_{ij} \sim \mathcal{N}(0, \ell^2)$ ,  $b_i \sim \mathcal{U}_{[0, 2\pi]}$ ,  $i \in [1, D]$ . We discuss some alternate approaches in Appendix A.1.

This embedding enjoys some nice properties. One such property is that,

$$\frac{2\langle \mathbf{B}_{\mathcal{F}}(x), \mathbf{B}_{\mathcal{F}}(x') \rangle}{D} \rightarrow \exp\left(\frac{-\ell^2 \|x - x'\|_2^2}{2}\right), \text{ as } D \rightarrow \infty.$$

This can be seen by recognizing that the Fourier transform of a Gaussian is Gaussian, with inverse variance. Note that natural coordinates, nor any affine transform thereof, behave in this way.

Further, for  $D \gg 1$ , the metamer problem is solved. As an informal proof we will consider the Gaussian limit above. For two coordinates sufficiently<sup>3</sup> distant from each other, their correlation will go to 0. This also holds true for their mean. However the mean of their embeddings must, for obvious reasons, be correlated with both embeddings. Hence the mean embedding and embedding mean must be distinguishable. This argument can easily be generalized to arbitrary numbers of points, and any other embeddings that enjoy rapidly decreasing correlation.

**Vector-Valued GPs** While GPs are often assumed to output scalar functions, extending them to the vector-valued case is not difficult. We choose the common assumption (Álvarez et al., 2012) that the output dimensions are uncorrelated, which makes the kernel block diagonal, and simplifies the resulting calculations in practice.

**Choice of Kernel** We follow Liu et al. (2021) and choose an exponential cosine similarity kernel. This kernel is defined as

$$K(x, y) = \exp\left(\tau^{-1} \frac{\langle x, y \rangle}{\sqrt{\langle x, x \rangle \langle y, y \rangle} + \varepsilon}\right).$$

We initialize  $\tau = 0.2$  and let it be fixed. We set  $\varepsilon = 10^{-6}$ . We found that letting the kernel be learnable had little effect on the performance, and that our method was robust to initializations between  $[0.1, 0.3]$ .

### 3.3. Decoding $\Lambda$ with $D$

When constructing  $\Lambda$ , the main assumption was that the mapping between images could be thought of as a feature to coordinate mapping, independent of the local neighbourhood. Here we want to construct a *decoder* that takes the local image structure into account, and additionally converts the coordinate embeddings back into natural coordinates. As previously mentioned, we choose to parametrize the image grid as  $[-1, 1] \times [-1, 1]$  and let the decoder predict a

<sup>3</sup>The exact distance of separation needed for non-ambiguity, under some assumption of noise, is often called the *metameric distance*.

single unconstrained coordinate<sup>4</sup>. We additionally let the decoder predict a confidence logit, for the predicted validity of the match. The input to the decoder is a combination of the encoded predicted coordinates from the GP, as well as local features in the query image. The architecture of the decoder is inspired by the decoder proposed by Yu et al. (2018), however there it was used for semantic segmentation.

**Convolutional Refinement** Once the embeddings have been decoded, we warp the support image to align with the query. After warping, we use convolutional regressive refiners, similar to Zhou et al. (2021), that predict relative offsets to both the predicted warp and the confidence in a multi-scale fashion. The refiners take the stacked features of the query image and the predicted aligned support image, and process both jointly. However, while Zhou et al. (2021) refine patches sparsely, we apply the refinement densely by using the estimated dense flow.

### 3.4. Loss Formulation

Our regression loss is

$$\mathcal{L}_{\text{warp}}(\hat{\omega}) = \|p(\mathbf{X}_{\mathcal{Q}}) \odot \|\omega(\mathbf{X}_{\mathcal{Q}}) - \hat{\omega}(\mathbf{X}_{\mathcal{Q}})\|_2\|_1.$$

The reference warps can come from projected depths like in (Sarlin et al., 2020; Sun et al., 2021) or from synthetic homographies, and the reference confidence  $p$  indicates, e.g., covisibility or consistent depth.

We further use a confidence loss,

$$\mathcal{L}_{\text{conf}}(\hat{p}) = \text{CE}(\hat{p}, p).$$

The final loss is,

$$\mathcal{L} = \mathcal{L}_{\text{warp}}(\hat{\omega}) + \lambda \mathcal{L}_{\text{conf}}(\hat{p}).$$

Where  $\lambda = 0.01$  is a balancing term. We follow previous work (Shen et al., 2020; Sarlin et al., 2020; Truong et al., 2021b) and produce losses for each scale. Like previous works (Zhou et al., 2021), we set  $p$  in the fine scale loss to 0 whenever the coarse scale warp is outside a threshold distance from the ground truth.

## 4. Experiments

### 4.1. Datasets

**MegaDepth** (Li & Snavely, 2018) is a large scale dataset, consisting of Structure from Motion (SfM) reconstructions of 196 different locations in the world. Importantly for our purposes, it contains depth maps computed from Multi View Stereo (MVS) which can be used to produce semi-dense reference warps for realistic scenes.

<sup>4</sup>Predictions outside the grid are naturally interpreted as lying on the extended image plane.

**HPatches** (Balntas et al., 2017) depicts planar scenes divided in sequences, with transformations restricted to homographies. Each image sequence contains a query image and 5 reference images taken under increasingly large viewpoints or illumination changes.

**YFCC100m** (Thomee et al., 2016) is a subset of the phototourism (Snavely et al., 2006; 2008) dataset with reference Bundler SfM reconstructions. We use this dataset to evaluate our approach for pose estimation.

### 4.2. Metrics

**PCK- $\tau$**  is defined as the proportion of the correspondences between the query and support image that are less than some threshold  $\tau$  away from the ground truth correspondences in the support image, i.e.

$$P(\|\hat{\omega} - \omega\|_2 < \tau).$$

**AEPE (Average End Point Error)** is defined as the *average* pixel error in the support image, and is hence quite similar to PCK. It is defined as

$$\mathbb{E}_x [\|\hat{\omega}(x) - \omega(x)\|_2].$$

For flows we set  $p(x) \propto \begin{cases} 1, & \omega(x) \text{ is valid,} \\ 0, & \text{else.} \end{cases}$

For sparse correspondences  $p(x)$  is typically dirac-deltas on the predicted sparse-correspondences, which can be obtained through, e.g., mutual nearest neighbours.

**AUC@ $\alpha$**  is defined as the integral of precision up to  $\alpha$ . Since the number of points is in practice finite, we follow the method by Truong et al. (2021b) and approximate the integral using the composite trapezoidal rule.

**mAP@ $\alpha$**  is defined as by Zhang et al. (2019) as the average of precision up to  $\alpha$ , with the average only being taken on the values [5, 10, 20]. This typically gives higher results than AUC, since the mAP@5 is the same as the accuracy.

**Pose Error** For YFCC100m, following previous work (Zhang et al., 2019) we use the pose error which is defined as the maximum angular error of both the estimated rotation and translation. The angular error of the estimated rotation is defined as

$$e_R(\hat{R}) = \left| \cos^{-1} \left( \frac{\text{tr}(R^\top \hat{R}) - 1}{2} \right) \right|,$$

and the angular error of the translation is the cosine similarity,

$$e_t(\hat{t}) = \frac{\langle t, \hat{t} \rangle}{\sqrt{\langle t, t \rangle \langle \hat{t}, \hat{t} \rangle}}.$$

With the combined error being

$$e(\hat{R}, \hat{t}) = \max(e_R(\hat{R}), e_t(\hat{t})).$$

### 4.3. Implementation Details

**Architecture** We use GPs on both scale 32 and 16 features of the backbone. We use 256 channels for the coordinate embedding, and use an internal dimension of 384 in our decoder. At scale 16 and up we use the convolutional refiners. Each convolutional refiner consists of 5 blocks, consisting of a  $5 \times 5$  depthwise separable convolution followed by batch norm (Ioffe & Szegedy, 2015), ReLU (Nair & Hinton, 2010), and a  $1 \times 1$  convolution. We do not use residual connections between the blocks.

**Training** Following Truong et al. (2021b) we train jointly on synthetic data and MegaDepth. However, while Truong et al. (2021b) use a sophisticated data generation process, with multiple independent moving objects and deformable transformations (Melekhov et al., 2019), we use a simpler generation method of only synthetic homographies with photometric distortions. For MegaDepth we do not perform any data augmentation. For both datasets we resize the images to a fixed resolution of  $384 \times 512$ .

We use a batch size of 32 and train for 200 000 gradient update steps with the AdamW (Loshchilov & Hutter, 2019) optimizer, with a learning rate of  $10^{-4}$  for the decoder, and  $10^{-6}$  for the backbone, and a weight-decay factor of  $10^{-4}$ . As backbone we use a ResNet50 (He et al., 2016) pretrained on ImageNet-1K (Russakovsky et al., 2015).

**Evaluation** We evaluate with the same image size as used during training. Following previous work (Truong et al., 2021b) we clip all matches to lie inside the image grid. We use the same model both for dense matching, sparse matching, and outdoor pose estimation.

### 4.4. Results

**Dense HPatches** For dense matching on HPatches we follow Melekhov et al. (2019) and Truong et al. (2020a), and evaluate only on the sequences in HPatches which contain changes in viewpoint. We resize the predictions bilinearly to the original image size and apply the scale 1 refiner. Our results are presented in Table 1. Our model greatly outperforms all previous single pass methods, achieving a 4% gain in PCK compared to the previous best method PDCNet. Impressively, our model even matches the performance of previous multiple pass methods which use orders of magnitude more computation.

**Sparse HPatches** While our main focus is dense geometric matching, we additionally evaluate on a sparse matching task on HPatches (Balntas et al., 2017). We use two different versions of our method. In one, we use the same procedure as for Dense HPatches and select the 2 000 most confident matches. In the second one, we additionally perform soft mutual nearest neighbour matching by filtering based on forward backward consistency. Notably, as can be seen in

Table 1. Dense Evaluation on HPatches. The top portion contains multiple-pass methods, while the lower portion contains single pass methods. We evaluate the flow in original image size. <sup>†</sup>COTR produces a single match at a time, hence computing a dense flow is multiple orders of magnitude slower than a single pass. <sup>1</sup>(Truong et al., 2021b), <sup>2</sup>(Jiang et al., 2021), <sup>3</sup>(Melekhov et al., 2019), <sup>4</sup>(Truong et al., 2020a)

	AEPE ↓	Dense HPatches		
		PCK ↑ @1px	PCK ↑ @3px	PCK ↑ @5px
PDCNet <sup>1</sup> CVPR'21	17.51	<b>48.69</b>	<b>82.71</b>	89.44
COTR <sup>†2</sup> ICCV'21	<b>7.75</b>	40.91	82.37	<b>91.10</b>
DGC-Net <sup>3</sup> WACV'19	33.26	12.00	-	58.06
GOCor <sup>4</sup> NeurIPS'20	20.16	41.49	74.12	81.46
PDCNet CVPR'21	19.40	43.94	78.51	85.81
<b>DKM</b>	<b>18.28</b>	<b>47.87</b>	<b>81.65</b>	<b>89.24</b>

Table 2. Sparse Evaluation on HPatches. The top portion contains sparse methods, while the lower portion contains dense methods. For DKM we select the 2 000 most confident matches. Note that some previous methods may output fewer matches, sometimes as low as a single match. <sup>1</sup>(Rocco et al., 2020), <sup>2</sup>(Sarlin et al., 2020), <sup>3</sup>(Wang et al., 2021), <sup>4</sup>(Tinchev et al., 2020)

	AEPE ↓	Sparse HPatches		
		PCK ↑ @1px	PCK ↑ @3px	PCK ↑ @5px
Sparse-NCNet <sup>1</sup> CVPR'20	44.65	78.52	86.95	
SuperGlue <sup>2</sup> CVPR'20	48.27	89.94	96.66	
DualRC-Net <sup>3</sup> NeurIPS'20	50.27	79.07	92.51	
XRCNet <sup>4</sup>	48.39	76.61	87.38	
<b>DKM</b>	<b>72.13</b>	<b>95.11</b>	<b>97.55</b>	
<b>DKM</b> (Soft Mutual Nearest)	<b>72.33</b>	<b>95.36</b>	<b>97.73</b>	

Table 2, our results are far superior to previous methods. In particular for low pixel thresholds where we achieve a 24.6% absolute gain in PCK-1. This indicates that sparse methods, which must first detect and then match, are unable to match the pixel-level precision of our dense method. Notably, while achieving extremely accurate matches, our method is also able to match the robustness of sparse methods, outperforming SuperGlue at the 5-pixel threshold.

**YFCC100m** We additionally evaluate our approach on the pose estimation benchmark YFCC100m (Thomee et al., 2016). For comparability we use the pairs provided by Zhang et al. (2019). We use the same approach as Truong et al. (2021b), and report both mAP as by Zhang et al. (2019) and AUC. To extract sparse matches, we randomly sample matches, up to a maximum of 20 000 matches. From our results in Table 3 it is clear that our method produces signif-

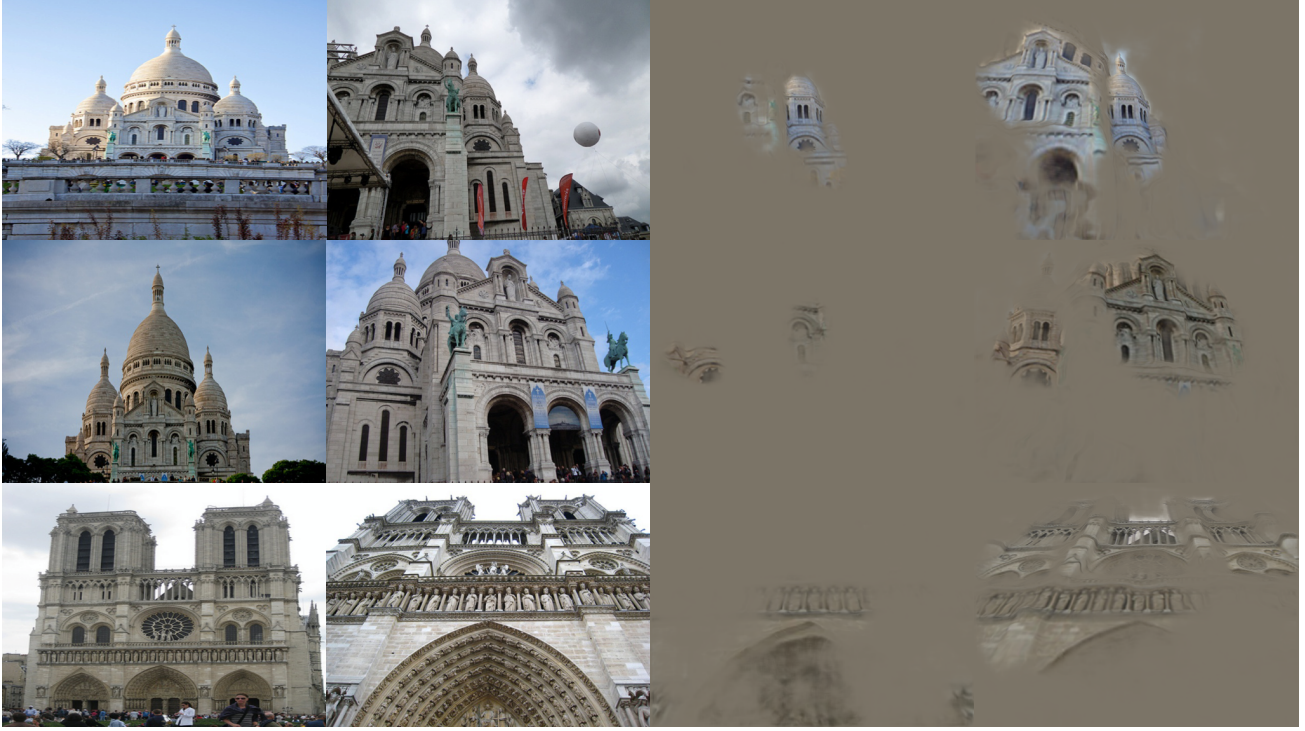


Figure 2. Qualitative results of our approach on pairs with extreme changes in viewpoint. We visualize the predicted alignment by multiplying it with the predicted confidence of the network. From left to right: Support image, query image, DKM without spatial embeddings, and our full method. Impressively, DKM is capable of both predicting extremely accurate correspondences, and simultaneously provide trustworthy confidence estimates.

icantly improved results compared to previous approaches. For single pass methods, our approach increases the AUC and mAP with about 4%. Additionally, we are able to outperform all previous multiple pass approaches.

#### 4.5. Ablation Study

In this section we investigate the effect of key components in our approach. We evaluate on our test split of MegaDepth, consisting of 4 scenes, and HPatches. Note that we consider the *forward* error, i.e. the same as sparse methods on HPatches, instead of the backward error as in Table 1. We present our results in Table 4.

**I – Fully Convolutional** As baseline we compare our method minus the global matching module. For a fair comparison, we add a convolutional module at stride 32. As expected this version performs the worst, owing to the difficulty of estimating large displacements.

**II – Identity Embedding** Instead of using a non-linear embedding, we instead use the GP to predict 2D coordinates directly. This version also performs poorly, giving significantly worse results than the full method. Hence it is clear that high-dimensional embeddings are crucial to distinguish

the multimodal matches from the intermediate match.

**III – No Coherency** Here we remove coherency information from the decoder by limiting the kernel size to 1. Since the decoder can only process pointwise correspondences, the performance is degraded as expected. The effect is especially large on HPatches, where the neighbourhood should give particularly strong information. This highlights the importance of local coherence when decoding the spatial embeddings.

**IV – Cross-Attention** We replace the GP to a cross-attention implementation using the same kernel. Here we also find a decrease in performance, indicating that the kernel-smoother approach is not able to produce the same level of accuracy as the GP. Here the performance is particularly effected on our Megadepth test split. Our intuition is that the attention kernel is able to model smooth coordinate transitions well, such as for planar scenes, but fails in scenes with depth discontinuities.

#### 4.6. Qualitative Examples

In Figure 2 we give qualitative examples for the performance of our approach for scenes with extreme changes in

Table 3. Pose estimation results on the YFCC100m benchmark, measured in AUC (higher is better). The top portion contains multiple pass methods, while the lower portion contains single pass methods. <sup>1</sup>(Shen et al., 2020), <sup>2</sup>(Zhang et al., 2019), <sup>3</sup>(Wiles et al., 2021)

	YFCC100m					
	Pose est. AUC $\uparrow$			Pose est. mAP $\uparrow$		
	@5°	@10°	@20°	@5°	@10°	@20°
RANSAC-Flow <sup>1</sup> <small>ECCV'20</small>	-	-	-	64.88	73.31	81.56
PDC-Net <small>CVPR'21</small>	35.71	55.81	72.26	63.90	73.00	81.22
OANet <sup>2</sup> <small>ICCV'19</small>	-	-	-	52.18	-	-
CoAM <sup>3</sup> <small>CVPR'21</small>	-	-	-	55.58	66.79	-
PDC-Net <small>CVPR'21</small>	32.21	52.61	70.13	60.52	70.91	80.30
<b>DKM</b>	<b>36.89</b>	<b>57.48</b>	<b>74.22</b>	<b>66.85</b>	<b>75.94</b>	<b>84.38</b>

Table 4. Ablation Study. Forward Dense Evaluation on HPatches and on our test split of MegaDepth. On HPatches we evaluate the flow in original image size, while on MegaDepth we evaluate in  $384 \times 512$  resolution.

	Forward Dense HPatches						Dense MegaDepth		
	AEPE $\downarrow$	PCK $\uparrow$			AEPE $\downarrow$	PCK $\uparrow$			
		@1px	@3px	@5px		@1px	@3px	@5px	
Fully Convolutional	26.19	50.49	76.22	81.45	36.95	40.28	56.86	61.86	
No Spatial Embedding	22.03	51.39	77.89	83.11	33.78	40.21	56.06	61.13	
No coherency	15.26	53.04	81.16	86.70	<u>28.19</u>	<u>45.34</u>	<u>63.46</u>	<u>69.16</u>	
Cross-Attention	<u>14.10</u>	<u>55.58</u>	<u>83.39</u>	<u>88.72</u>	31.90	41.56	59.81	65.15	
<b>DKM</b>	<b>12.71</b>	<b>56.28</b>	<b>84.41</b>	<b>89.85</b>	<b>28.06</b>	<b>45.35</b>	<b>64.80</b>	<b>70.46</b>	

viewpoint. For comparison we additionally show the performance of our model without the coordinate embeddings. Notably, our approach is able to predict accurate and reliable dense correspondences even for these extreme cases, while the naive regression approach often fails completely.

## 5. Conclusion

In this paper we formulated a unique approach to global correlation and correspondence extraction by posing it as a feature-vector to coordinate probabilistic regression task. We extended the regression task to embedded coordinate spaces, yielding both improvements in performance and insights. Finally, we proposed an embedded coordinate decoder and a multiscale refinement module which gave sub-pixel performance. Our proposed method achieved impressive improvements of 4% AUC@5° on the YFCC100m pose estimation benchmark, and a 4% PCK-1 improvement on dense HPatches and a remarkable gain of over 20% PCK-1 on sparse HPatches.

Besides setting a new state-of-the-art on learning dense geometric matching, our findings might also have impact on other problems that combine displacement/vector fields and feature spaces, such as hyper-spectral measurements from satellites for climate monitoring. Furthermore, the

combination of GPs with embedded coordinate spaces to generate multi-modal responses might be applicable to many other domains where GPs were previously less suitable.

## Acknowledgements

This work was partially supported by the Wallenberg Artificial Intelligence, Autonomous Systems and Software Program (WASP) funded by Knut and Alice Wallenberg Foundation; and by the strategic research environment ELLIIT funded by the Swedish government. The computations were enabled by resources provided by the Swedish National Infrastructure for Computing (SNIC), partially funded by the Swedish Research Council through grant agreement no. 2018-05973.

## References

Adelson, E. H. and Movshon, J. A. Phenomenal coherence of moving visual patterns. *Nature*, 300(5892):523–525, 1982.

Balntas, V., Lenc, K., Vedaldi, A., and Mikolajczyk, K. Hpatches: A benchmark and evaluation of handcrafted and learned local descriptors. In *Proceedings of the IEEE conference on computer vision and pattern recognition*, pp. 5173–5182, 2017.

Bay, H., Tuytelaars, T., and Van Gool, L. Surf: Speeded up robust features. In *European conference on computer vision*, pp. 404–417. Springer, 2006.

Bian, J., Lin, W.-Y., Matsushita, Y., Yeung, S.-K., Nguyen, T.-D., and Cheng, M.-M. Gms: Grid-based motion statistics for fast, ultra-robust feature correspondence. In *Proceedings of the IEEE Conference on Computer Vision and Pattern Recognition (CVPR)*, July 2017.

Black, M. J. and Anandan, P. The robust estimation of multiple motions: Parametric and piecewise-smooth flow fields. *Computer vision and image understanding*, 63(1):75–104, 1996.

Brachmann, E. and Rother, C. Neural-guided ransac: Learning where to sample model hypotheses. In *Proceedings of the IEEE/CVF International Conference on Computer Vision*, pp. 4322–4331, 2019.

Brox, T. and Malik, J. Large displacement optical flow: descriptor matching in variational motion estimation. *IEEE transactions on pattern analysis and machine intelligence*, 33(3):500–513, 2010.

Campbell, F. W. and Robson, J. G. Application of fourier analysis to the visibility of gratings. *The Journal of physiology*, 197(3):551–566, 1968.

Dalal, N. and Triggs, B. Histograms of oriented gradients for human detection. In *2005 IEEE computer society conference on computer vision and pattern recognition (CVPR'05)*, volume 1, pp. 886–893. Ieee, 2005.

DeTone, D., Malisiewicz, T., and Rabinovich, A. Superpoint: Self-supervised interest point detection and description. In *Proceedings of the IEEE conference on computer vision and pattern recognition workshops*, pp. 224–236, 2018.

Dosovitskiy, A., Fischer, P., Ilg, E., Hausser, P., Hazirbas, C., Golkov, V., Van Der Smagt, P., Cremers, D., and Brox, T. Flownet: Learning optical flow with convolutional networks. In *Proceedings of the IEEE international conference on computer vision*, pp. 2758–2766, 2015.

Dusmanu, M., Rocco, I., Pajdla, T., Pollefeys, M., Sivic, J., Torii, A., and Sattler, T. D2-Net: A Trainable CNN for Joint Detection and Description of Local Features. In *Proceedings of the 2019 IEEE/CVF Conference on Computer Vision and Pattern Recognition*, 2019.

Felsberg, M., Larsson, F., Wiklund, J., Wadstromer, N., and Ahlberg, J. Online learning of correspondences between images. *IEEE transactions on pattern analysis and machine intelligence*, 35(1):118–129, 2012.

Forssén, P.-E. *Low and medium level vision using channel representations*. PhD thesis, Linköping University Electronic Press, 2004.

Friedman, J., Hastie, T., Tibshirani, R., et al. *The elements of statistical learning*, volume 1. Springer series in statistics New York, 2001.

Häger, G., Persson, M., and Felsberg, M. Predicting disparity distributions. In *2021 IEEE International Conference on Robotics and Automation (ICRA)*, pp. 4363–4369. IEEE, 2021.

He, K., Zhang, X., Ren, S., and Sun, J. Deep residual learning for image recognition. In *Proceedings of the IEEE conference on computer vision and pattern recognition*, pp. 770–778, 2016.

Horn, B. K. and Schunck, B. G. Determining optical flow. *Artificial intelligence*, 17(1-3):185–203, 1981.

Huang, Z., Pan, X., Xu, R., Xu, Y., Zhang, G., Li, H., et al. Life: Lighting invariant flow estimation. *arXiv preprint arXiv:2104.03097*, 2021.

Hur, J. and Roth, S. Optical flow estimation in the deep learning age. In *Modelling Human Motion*, pp. 119–140. Springer, 2020.

Ilg, E., Mayer, N., Saikia, T., Keuper, M., Dosovitskiy, A., and Brox, T. Flownet 2.0: Evolution of optical flow estimation with deep networks. In *Proceedings of the IEEE conference on computer vision and pattern recognition*, pp. 2462–2470, 2017.

Ioffe, S. and Szegedy, C. Batch normalization: Accelerating deep network training by reducing internal covariate shift. In *International conference on machine learning*, pp. 448–456. PMLR, 2015.

Jiang, W., Trulls, E., Hosang, J., Tagliasacchi, A., and Yi, K. M. COTR: Correspondence Transformer for Matching Across Images. In *ICCV*, 2021.

Johnander, J., Edstedt, J., Felsberg, M., Khan, F. S., and Danelljan, M. Dense gaussian processes for few-shot segmentation. *arXiv preprint arXiv:2110.03674*, 2021.

Jonsson, E. and Felsberg, M. Efficient computation of channel-coded feature maps through piecewise polynomials. *Image and Vision Computing*, 27(11):1688–1694, 2009.

Kim, S., Min, D., Jeong, S., Kim, S., Jeon, S., and Sohn, K. Semantic attribute matching networks. In *Proceedings of the IEEE/CVF Conference on Computer Vision and Pattern Recognition*, pp. 12339–12348, 2019.

Laskar, Z., Melekhov, I., Tavakoli, H. R., Ylioinas, J., and Kannala, J. Geometric image correspondence verification by dense pixel matching. In *Proceedings of the IEEE/CVF Winter Conference on Applications of Computer Vision*, pp. 2521–2530, 2020.

Li, S., Han, K., Costain, T. W., Howard-Jenkins, H., and Prisacariu, V. Correspondence networks with adaptive neighbourhood consensus. In *Proceedings of the IEEE/CVF Conference on Computer Vision and Pattern Recognition*, pp. 10196–10205, 2020.

Li, Z. and Snavely, N. Megadepth: Learning single-view depth prediction from internet photos. In *Proceedings of the IEEE Conference on Computer Vision and Pattern Recognition*, pp. 2041–2050, 2018.

Liu, C., Yuen, J., and Torralba, A. Sift flow: Dense correspondence across scenes and its applications. *IEEE transactions on pattern analysis and machine intelligence*, 33(5):978–994, 2010.

Liu, Z., Hu, H., Lin, Y., Yao, Z., Xie, Z., Wei, Y., Ning, J., Cao, Y., Zhang, Z., Dong, L., et al. Swin transformer v2: Scaling up capacity and resolution. *arXiv preprint arXiv:2111.09883*, 2021.

Loshchilov, I. and Hutter, F. Decoupled weight decay regularization. In *International Conference on Learning Representations*, 2019. URL <https://openreview.net/forum?id=Bkg6RiCqY7>.

Lowe, D. G. Distinctive image features from scale-invariant keypoints. *International journal of computer vision*, 60(2):91–110, 2004.

Lucas, B. D. and Kanade, T. An iterative image registration technique with an application to stereo vision. In *Proceedings of the 7th International Joint Conference on Artificial Intelligence - Volume 2*, IJCAI’81, pp. 674–679, 1981.

Luo, Z., Shen, T., Zhou, L., Zhang, J., Yao, Y., Li, S., Fang, T., and Quan, L. Contextdesc: Local descriptor augmentation with cross-modality context. In *Proceedings of the IEEE/CVF Conference on Computer Vision and Pattern Recognition*, pp. 2527–2536, 2019.

Lynen, S., Zeisl, B., Aiger, D., Bosse, M., Hesch, J., Pollefeys, M., Siegwart, R., and Sattler, T. Large-scale, real-time visual-inertial localization revisited. *The International Journal of Robotics Research*, 39(9):1061–1084, 2020.

Ma, J., Zhao, J., Tian, J., Yuille, A. L., and Tu, Z. Robust point matching via vector field consensus. *IEEE Transactions on Image Processing*, 23(4):1706–1721, 2014.

Melekhov, I., Tiulpin, A., Sattler, T., Pollefeys, M., Rahtu, E., and Kannala, J. Dgc-net: Dense geometric correspondence network. In *2019 IEEE Winter Conference on Applications of Computer Vision (WACV)*, pp. 1034–1042. IEEE, 2019.

Mur-Artal, R., Montiel, J. M. M., and Tardos, J. D. Orb-slam: a versatile and accurate monocular slam system. *IEEE transactions on robotics*, 31(5):1147–1163, 2015.

Nair, V. and Hinton, G. E. Rectified linear units improve restricted boltzmann machines. In *ICML*, 2010.

Nordberg, K., Granlund, G., and Knutsson, H. Representation and learning of invariance. In *Proceedings of 1st International Conference on Image Processing*, volume 2, pp. 585–589. IEEE, 1994.

Patacchiola, M., Turner, J., Crowley, E. J., and Storkey, A. Bayesian meta-learning for the few-shot setting via deep kernels. In *Advances in Neural Information Processing Systems*, 2020.

Pouget, A., Dayan, P., and Zemel, R. Information processing with population codes. *Nature Reviews Neuroscience*, 1(2):125–132, 2000.

Rahimi, A. and Recht, B. Random features for large-scale kernel machines. In *Proceedings of the 20th International Conference on Neural Information Processing Systems*, NIPS’07, pp. 1177–1184, 2007.

Rasmussen, C. E. and Williams, C. K. I. *Gaussian Processes for Machine Learning (Adaptive Computation and Machine Learning)*. The MIT Press, 2005. ISBN 026218253X.

Revaud, J., De Souza, C., Humenberger, M., and Weinzaepfel, P. R2d2: Reliable and repeatable detector and descriptor. *Advances in neural information processing systems*, 32:12405–12415, 2019.

Rocco, I., Arandjelovic, R., and Sivic, J. Convolutional neural network architecture for geometric matching. In *Proceedings of the IEEE conference on computer vision and pattern recognition*, pp. 6148–6157, 2017.

Rocco, I., Cimpoi, M., Arandjelović, R., Torii, A., Pajdla, T., and Sivic, J. Neighbourhood consensus networks. In *Proceedings of the 32nd Conference on Neural Information Processing Systems*, 2018.

Rocco, I., Arandjelović, R., and Sivic, J. Efficient neighbourhood consensus networks via submanifold sparse convolutions. In *European Conference on Computer Vision*, pp. 605–621. Springer, 2020.

Russakovsky, O., Deng, J., Su, H., Krause, J., Satheesh, S., Ma, S., Huang, Z., Karpathy, A., Khosla, A., Bernstein, M., et al. Imagenet large scale visual recognition challenge. *International journal of computer vision*, 115(3): 211–252, 2015.

Sarlin, P.-E., DeTone, D., Malisiewicz, T., and Rabinovich, A. Superglue: Learning feature matching with graph neural networks. In *Proceedings of the IEEE/CVF conference on computer vision and pattern recognition*, pp. 4938–4947, 2020.

Schonberger, J. L. and Frahm, J.-M. Structure-from-motion revisited. In *Proceedings of the IEEE conference on computer vision and pattern recognition*, pp. 4104–4113, 2016.

Shen, X., Darmon, F., Efros, A. A., and Aubry, M. Ransac-flow: generic two-stage image alignment. In *Computer Vision–ECCV 2020: 16th European Conference, Glasgow, UK, August 23–28, 2020, Proceedings, Part IV 16*, pp. 618–637. Springer, 2020.

Shrivastava, A., Malisiewicz, T., Gupta, A., and Efros, A. A. Data-driven visual similarity for cross-domain image matching. In *Proceedings of the 2011 SIGGRAPH Asia Conference*, pp. 1–10, 2011.

Snavely, N., Seitz, S. M., and Szeliski, R. Photo tourism: exploring photo collections in 3d. In *ACM siggraph 2006 papers*, pp. 835–846. 2006.

Snavely, N., Seitz, S. M., and Szeliski, R. Modeling the world from internet photo collections. *International journal of computer vision*, 80(2):189–210, 2008.

Snell, J. and Zemel, R. Bayesian few-shot classification with one-vs-each pôlya-gamma augmented gaussian processes. In *International Conference on Learning Representations*, 2021.

Snippe, H. P. and Koenderink, J. J. Discrimination thresholds for channel-coded systems. *Biological cybernetics*, 66(6):543–551, 1992.

Sun, D., Yang, X., Liu, M.-Y., and Kautz, J. Pwc-net: Cnns for optical flow using pyramid, warping, and cost volume. In *Proceedings of the IEEE conference on computer vision and pattern recognition*, pp. 8934–8943, 2018.

Sun, J., Shen, Z., Wang, Y., Bao, H., and Zhou, X. Loftr: Detector-free local feature matching with transformers. In *Proceedings of the IEEE/CVF Conference on Computer Vision and Pattern Recognition*, pp. 8922–8931, 2021.

Tancik, M., Srinivasan, P. P., Mildenhall, B., Fridovich-Keil, S., Raghavan, N., Singhal, U., Ramamoorthi, R., Barron, J. T., and Ng, R. Fourier features let networks learn high frequency functions in low dimensional domains. In *Advances in Neural Information Processing Systems 33: Annual Conference on Neural Information Processing Systems 2020, NeurIPS 2020, December 6-12, 2020, virtual*.

Teed, Z. and Deng, J. Raft: Recurrent all-pairs field transforms for optical flow. In *European conference on computer vision*, pp. 402–419. Springer, 2020.

Thomee, B., Shamma, D. A., Friedland, G., Elizalde, B., Ni, K., Poland, D., Borth, D., and Li, L.-J. Yfcc100m: The new data in multimedia research. *Communications of the ACM*, 59(2):64–73, 2016.

Tinchev, G., Li, S., Han, K., Mitchell, D., and Kouskouridas, R. Xresolution correspondence networks. *arXiv preprint arXiv:2012.09842*, 2020.

Toft, C., Maddern, W., Torii, A., Hammarstrand, L., Stenborg, E., Safari, D., Okutomi, M., Pollefeys, M., Sivic, J., Pajdla, T., et al. Long-term visual localization revisited. *IEEE Transactions on Pattern Analysis and Machine Intelligence*, 2020.

Truong, P., Danelljan, M., Gool, L. V., and Timofte, R. Gocor: Bringing globally optimized correspondence volumes into your neural network. *Advances in Neural Information Processing Systems*, 33, 2020a.

Truong, P., Danelljan, M., and Timofte, R. Glu-net: Global-local universal network for dense flow and correspondences. In *Proceedings of the IEEE/CVF conference on computer vision and pattern recognition*, pp. 6258–6268, 2020b.

Truong, P., Danelljan, M., Timofte, R., and Van Gool, L. Pdc-net+: Enhanced probabilistic dense correspondence network. *arXiv preprint arXiv:2109.13912*, 2021a.

Truong, P., Danelljan, M., Van Gool, L., and Timofte, R. Learning accurate dense correspondences and when to trust them. In *Proceedings of the IEEE/CVF Conference on Computer Vision and Pattern Recognition*, pp. 5714–5724, 2021b.

Truong, P., Danelljan, M., Yu, F., and Gool, L. V. Warp consistency for unsupervised learning of dense correspondences. In *IEEE/CVF International Conference on Computer Vision, ICCV*, 2021c.

Tsai, Y.-H. H., Bai, S., Yamada, M., Morency, L.-P., and Salakhutdinov, R. Transformer dissection: An unified understanding for transformer's attention via the lens of kernel. In *Proceedings of the 2019 Conference on Empirical Methods in Natural Language Processing and the 9th International Joint Conference on Natural Language Processing (EMNLP-IJCNLP)*, pp. 4344–4353, Hong Kong, China, November 2019. Association for Computational Linguistics.

Tyszkiewicz, M. J., Fua, P., and Trulls, E. DISK: learning local features with policy gradient. In *NeurIPS*, 2020.

Wallach, H. Über visuell wahrgenommene bewegungsrichtung. *Psychologische Forschung*, 20(1):325–380, 1935.

Wang, Q., Zhou, X., Hariharan, B., and Snavely, N. Learning feature descriptors using camera pose supervision. In *Proc. European Conference on Computer Vision (ECCV)*, 2020.

Wang, Z., Miao, Z., Zhen, X., and Qiu, Q. Learning to learn dense gaussian processes for few-shot learning. *Advances in Neural Information Processing Systems*, 34, 2021.

Weiss, Y. and Adelson, E. H. Slow and smooth: A bayesian theory for the combination of local motion signals in human vision. *MIT AI Memo 1624*, 1998.

Wiles, O., Ehrhardt, S., and Zisserman, A. Co-attention for conditioned image matching. In *Proceedings of the IEEE/CVF Conference on Computer Vision and Pattern Recognition*, pp. 15920–15929, 2021.

Wilson, A. G., Hu, Z., Salakhutdinov, R., and Xing, E. P. Deep kernel learning. In *Artificial intelligence and statistics*, pp. 370–378. PMLR, 2016.

Wohlgemuth, A. *On the after-effect of seen movement*. Number 1-2. University Press, 1911.

Yi, K. M., Trulls, E., Ono, Y., Lepetit, V., Salzmann, M., and Fua, P. Learning to find good correspondences. In *Proceedings of the IEEE conference on computer vision and pattern recognition*, pp. 2666–2674, 2018.

Yu, C., Wang, J., Peng, C., Gao, C., Yu, G., and Sang, N. Learning a discriminative feature network for semantic segmentation. In *Proceedings of the IEEE conference on computer vision and pattern recognition*, pp. 1857–1866, 2018.

Yuille, A. L. and Grzywacz, N. M. A computational theory for the perception of coherent visual motion. *Nature*, 333 (6168):71–74, 1988.

Zhang, J., Sun, D., Luo, Z., Yao, A., Zhou, L., Shen, T., Chen, Y., Quan, L., and Liao, H. Learning two-view correspondences and geometry using order-aware network. *International Conference on Computer Vision (ICCV)*, 2019.

Zhou, Q., Sattler, T., and Leal-Taixe, L. Patch2pix: Epipolar-guided pixel-level correspondences. In *Proceedings of the IEEE/CVF Conference on Computer Vision and Pattern Recognition*, pp. 4669–4678, 2021.

Álvarez, M. A., Rosasco, L., and Lawrence, N. D. Kernels for vector-valued functions: A review. *Foundations and Trends® in Machine Learning*, 4(3):195–266, 2012. ISSN 1935-8237. doi: 10.1561/2200000036. URL <http://dx.doi.org/10.1561/2200000036>.

## A. Appendix

### A.1. Spatial Embeddings

Here we investigate some other choices of embeddings.

While fourier features in the limit make up a basis for the SE-kernel, we are free to choose another equivalent basis. One other such obvious choice is to use uniformly distributed SE-basis functions with the same length as the kernel. These functions can be written

$$\mathbf{B}_{SE}(y; \theta, \ell) = \exp\left(-\frac{\|y - \theta\|_2^2}{\ell^2}\right)$$

Note that, due to the non-compact support of the SE, we must choose some reasonable range to uniformly sample them. We sample uniformly from  $[-1 - \frac{1}{\ell}, 1 + \frac{1}{\ell}]$ . Hence we get,

$$\frac{\ell^2 \langle \mathbf{B}_{SE}(x), \mathbf{B}_{SE}(x') \rangle}{D} \rightarrow \exp(-\ell^2 \|x - x'\|_2^2), \text{ as } D \rightarrow \infty.$$

While the inner product has the same limit (with some scaling factor), this basis tends to be much sparser as  $\ell \rightarrow \infty$ , which might be desirable.

We can take the notion of basis sparsity even further with a compact support basis, e.g. the  $\cos^2$ -basis (Nordberg et al., 1994), which can be written as

$$\mathbf{B}_{\cos^2}(x; \theta, \ell) = \cos^2\left(\frac{\pi\|x - \theta\|_2}{\ell}\right) \left(\|x - \theta\|_2 < \frac{\ell}{2}\right).$$

An advantage with this kernel is that we only need to sample positions in a bounded region around  $[-1 - \ell\pi/2, 1 + \ell\pi/2]$ . The kernel implied by this function basis is somewhat cumbersome to write out. In 1-D it is given by

$$\begin{aligned} \langle \mathbf{B}_{\cos^2}(x), \mathbf{B}_{\cos^2}(x') \rangle &\propto \\ &[-(2 \sin(x + x' - 2\theta) - 4(\sin(2(x - \theta)) + 2 \sin(x' - \theta) - 2\theta) + 4\theta \cos(2(x - x'))) \rangle_{\max(x, x') - \pi/2}^{\min(x, x') + \pi/2}, \\ &\text{as } D \rightarrow \infty, \end{aligned}$$

Which while less practical to work with, is an interesting fact non-the-less. This basis is extremely sparse, especially for short length scales.

During initial experiments, we found that all these give almost identical results from training. This indicates that it is mostly the correlative structure of the embeddings that matters when choosing basis functions.

### A.2. Toy-Example

Here we provide some intuition for the statements in Section 3.2 by considering  $\Phi = [0, 1]$  and  $\mathbb{E} = \mathbb{R}$ . To illustrate the inherent global non-uniqueness of feature-vectors, and the varying density of observations, we sample from the following distribution:

$$p(x, y) = 0.8p_1(x, y) + 0.2p_2(x, y), \quad (1)$$

where,

$$\begin{cases} p_1(x, y) = \mathcal{N}(y; x, 0.1) \cdot \mathcal{U}_{[0, 0.5]}(x) \\ p_2(x, y) = \mathcal{N}(y; -x, 0.1) \cdot \mathcal{U}_{[0.4, 1.0]}(x) \end{cases}$$

For both cross-attention and the GP we will use a squared exponential kernel, i.e.

$$k(x, x') = \exp\left(-\frac{(x - x')^2}{\ell^2}\right),$$

with  $\ell = 0.1$ . We sample  $n = 100$  support points, and plot the results in Figure 3. From this simple example the previously discussed properties can clearly be seen. Notably, the slope of the GP around the discontinuity is much sharper, and less biased than the attention based smoother.

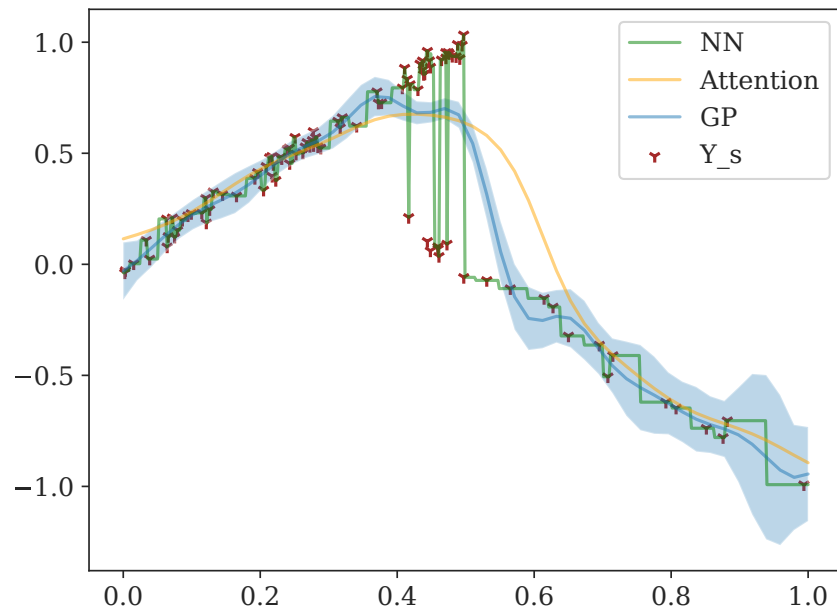


Figure 3. Comparative plot for the toy example of different inference approaches.